

Supporting information

**Energy transfer and formation of long-lived $^3\text{MLCT}$ states in multimetallic complexes
with extended highly conjugated bis-terpyridyl ligands**

Dr. Maria Wächtler,^a Joachim Kübel,^{a,b} Kevin Barthelmes,^{c,d} Dr. Andreas Winter,^{c,d}
Alexander Schmiedel,^e Dr. Torbjörn Pascher,^f Prof. Christoph Lambert,^e Prof. Ulrich S.
Schubert,^{c,d} Prof. Benjamin Dietzek^{a,b,d} *

AFFILITATIONS

a Leibniz Institute of Photonic Technology e.V., Albert-Einstein-Straße 9, 07745 Jena,
Germany

b Institute of Physical Chemistry and Abbe Center of Photonics, Friedrich Schiller University
Jena, Helmholtzweg 4, 07745 Jena, Germany

c Laboratory of Organic and Macromolecular Chemistry (IOMC), Friedrich Schiller
University Jena, Humboldtstraße 10, 07743 Jena, Germany

d Jena Center for Soft Matter (JCSM), Friedrich Schiller University Jena, Philosophenweg 7,
07743 Jena, Germany

e Institut für Organische Chemie, Universität Würzburg, Wilhelm Conrad Röntgen Research
Center for Complex Material Systems, Center for Nanosystems Chemistry, Am Hubland,
97074 Würzburg, Germany

f Pascher Instruments AB, Stora Råbybyaväg 24, 22478 Lund, Sweden

*corresponding author:

benjamin.dietzek@ipht-jena.de, phone +49 (0)3641 206-332, fax +49 (0)3641 206-390

Synthesis and characterization

All reagents were purchased from commercial sources and used without further purification unless specified. Chromatographic separation was performed with standardized silica gel 60 (Merck) and aluminum oxide 90 neutral (Molekula). The reaction progress was controlled by thin layer chromatography (TLC) using aluminum sheets precoated with silica gel 60 F254 and aluminum oxide 60 F254 neutral (Merck). Nuclear magnetic resonance (NMR) spectra were recorded on a AC 300 MHz (Bruker) spectrometer at 298 K. Chemical shifts are reported in parts per million (ppm, δ scale) relative to the residual signal of the deuterated solvent. Coupling constants are given in Hz. High resolution (HR) ESI-TOF MS was performed on an ESI-(Q)-TOF-MS MICROTOF II (Bruker Daltonics) mass spectrometer.

The Ligand **L**,¹ [Ru(tpy)(acetonitrile)₃](PF₆)₂,² and Os(tpy)Cl₃³ were prepared according to literature procedures.

Compound Ru

A microwave vial (20 mL) was charged with [Ru(tpy)(acetonitrile)₃](PF₆)₂ (44 mg, 59 μ mol), ditopic ligand **L** (103 mg, 71 μ mol) and DMF (10 mL). The vial was capped and purged with nitrogen for 20 min. The suspension was heated to 160 °C for 3 h in an oil bath. After cooling to room temperature, the reaction mixture was filtrated to remove the unreacted ligand. The filtrate was added to an aqueous ammonium hexafluorophosphate solution. The red precipitate was collected by filtration, washed with water, then methanol and diethyl ether. Subsequently, the solid was dissolved in acetone and loaded on a alumina column (dichloromethane/methanol, 95:5 ratio). The first dark red fraction was collected, concentrated *in vacuo* and precipitated in *n*-hexane. The compound was obtained as red solid (43 mg, 35%).

^1H NMR (300 MHz, CD_2Cl_2 , ppm): δ 8.91 (s, 2H), 8.80 (s, 2H), 8.74 (d, $J = 6.2$ Hz, 2H), 8.73 (d, $J = 7.9$ Hz, 2H), 8.70 (d, $J = 8.4$ Hz, 2H), 8.60 (d, $J = 8.2$ Hz, 2H), 8.47 (d, $J = 8.1$ Hz, 2H), 8.44 (t, $J = 8.2$ Hz, 1H), 8.18 (d, $J = 8.1$ Hz, 2H), 8.01–7.80 (m, 10H), 7.70 (d, $J = 7.9$ Hz, 2H), 7.58 (s, 4H), 7.55 (d, $J = 16.1$ Hz, 1H), 7.53 (d, $J = 16.2$ Hz, 1H), 7.44–7.36 (m, 4H), 7.33 (d, $J = 5.5$ Hz, 2H), 7.25 (d, $J = 16.3$ Hz, 2H), 7.24–7.18 (m, 6H), 7.12 (s, 1H), 7.08 (s, 1H), 4.24–3.97 (m, 8H), 2.06–1.77 (m, 8H), 1.72–1.15 (m, 40H), 1.01–0.71 (m, 12H) ppm.

HRMS (ESI-TOF, CH_3CN , m/z): 895.9145, $\text{C}_{115}\text{H}_{119}\text{N}_9\text{O}_4\text{Ru}$ ($[\text{M}-2\text{PF}_6]^{2+}$) requires 895.9211.

Compound RuOs

A microwave vial (2 mL) was charged with $\text{Os}(\text{tpy})\text{Cl}_3$ (3.5 mg, 6.63 μmol) and silver(I)-tetrafluoroborate (3.9 mg, 20 μmol) in acetone (3 mL). The vial was capped and purged with nitrogen for 20 min. The mixture was heated to 70 $^\circ\text{C}$ for 2 h. After cooling and filtration, DMAc/ethylene glycol (3:1, 2 mL) was added to the filtrate and the acetone was removed *in vacuo*. The resulting black solution was added to a microwave vial (2 mL) charged with **Ru** (11.5 mg, 5.52 μmol). The vial was capped and purged with nitrogen for 20 min. The mixture was heated to 160 $^\circ\text{C}$ for 24 h. Subsequently, the solution was cooled to room temperature and precipitated from an aqueous ammonium hexafluorophosphate solution. After filtration and washing with water, the crude product was purified by column chromatography (silica, $\text{CH}_3\text{CN}/\text{H}_2\text{O}/\text{sat. aq. KNO}_3$ 70:4:1 then 40:4:1 ratio). The dark brown fraction was concentrated and precipitated by adding an aqueous ammonium hexafluorophosphate solution to obtain a dark brown solid (8 mg, 51%).

^1H NMR (300 MHz, CD_3CN , ppm): δ 9.05 (s, 2H), 9.03 (s, 2H), 8.77 (d, $J = 8.6$ Hz, 2H), 8.76 (d, $J = 7.9$ Hz, 2H), 8.65 (d, $J = 7.0$ Hz, 2H), 8.63 (d, $J = 7.0$ Hz, 2H), 8.50 (d, $J = 7.6$ Hz, 2H), 8.48 (d, $J = 7.6$ Hz, 2H), 8.42 (t, $J = 8.2$ Hz, 1H), 8.24 (d, $J = 8.0$ Hz, 2H), 8.21 (d, J

= 8.5 Hz, 2H), 7.99–7.87 (m, 9H), 7.82 (d, $J = 8.5$ Hz, 2H), 7.77 (d, $J = 8.5$ Hz, 2H), 7.66–7.49 (m, 6H), 7.44 (d, $J = 5.7$ Hz, 2H), 7.39–7.34 (m, 2H), 7.35 (d, $J = 5.3$ Hz, 2H), 7.31 (d, $J = 5.9$ Hz, 2H), 7.23 (d, $J = 5.6$ Hz, 2H), 7.20 (s, 1H), 7.18 (d, $J = 6.2$ Hz, 4H), 7.16 (s, 1H), 7.13 (s, 1H), 7.11 (d, $J = 6.8$ Hz, 4H), 7.08 (s, 1H), 4.26–3.93 (m, 8H), 2.06–1.77 (m, 8H), 1.70–1.13 (m, 40H), 1.02–0.71 (m, 12H).

HRMS (ESI-TOF, CH_3CN , m/z): 554.2261, $\text{C}_{130}\text{H}_{130}\text{N}_{12}\text{O}_4\text{OsRu}$ ($[\text{M}-4\text{PF}_6]^{4+}$) requires 554.2252.

Compound RuFeRu

A microwave vial (2 mL) was charged with **Ru** (11.8 mg, 5.67 μmol) and dichloromethane (1.5 mL). The vial was capped and purged with nitrogen for 20 min. To the stirring solution was added iron(II)-sulfate heptahydrate (0.87 mg, 3.12 μmol) in methanol (0.5 mL) via a syringe. The resulting mixture continued stirring for 2 h. Subsequently, the solvents were removed by a stream of nitrogen and ammonium hexafluorophosphate (30 mg, 187 μmol), acetonitrile (3 mL) was added. After 15 min stirring at room temperature, water (30 mL) was added, to precipitate the complex. Subsequently, the suspension was filtrated and intensively washed with water to obtain a dark red-brown solid (12 mg, 85%).

^1H NMR (300 MHz, CD_3CN , ppm): δ 9.21 (s, 4H), 9.02 (s, 4H), 8.76 (d, $J = 8.1$ Hz, 4H), 8.69–8.60 (m, 8H), 8.50 (d, $J = 8.9$ Hz, 4H), 8.42 (t, $J = 7.6$ Hz, 2H), 8.38 (d, $J = 7.8$ Hz, 4H), 8.26 (d, $J = 7.8$ Hz, 4H), 8.01–7.84 (m, 20H), 7.64 (s, 8H), 7.57 (d, $J = 16.6$ Hz, 4H), 7.46–7.32 (m, 12H), 7.24–7.14 (m, 20H), 7.10 (dd, $J = 7.8, 7.1$ Hz, 4H), 4.25–4.16 (m, 8H), 4.15–4.06 (m, 8H), 2.05–1.82 (m, 16H), 1.69–1.16 (m, 80H), 1.03–0.76 (m, 24H).

HRMS (ESI-TOF, CH_3CN , m/z): 606.6051, $\text{C}_{230}\text{H}_{238}\text{FeN}_{18}\text{O}_8\text{Ru}_2$ ($[\text{M}-6\text{PF}_6]^{6+}$) requires 606.6043.

Experimental Section

The pump pulses for the ns time-resolved transient absorption measurements of **Ru** and **RuFeRu** at 520 nm were delivered by an OPO (OPO-PLUS, Continuum) pumped by a ND:YAG (Surelite S10 II, Continuum) laser at 10 Hz resulting in pulses with a duration of 5 ns. Probe light is delivered by a pulsed 75 W Xe arc lamp. The sample is probed in 90° geometry. Spherical concave mirrors were used to focus the probe light at the sample position and to refocus the light on the entrance slit of a monochromator (Acton, Princeton Instruments). Probe light is detected by a PMT (Hamamatsu R928) mounted on a fivestage base and the signal was processed by a commercially available detection system (Pascher Instruments AB). By switching off the probe light, emission decay can be detected with ns-temporal resolution.

For **Ru** and **RuFeRu** fs time-resolved transient absorption spectroscopy was performed on an experimental setup with maximum delay between pump and probe pulses of 8 ns. The laser system consists of an ultrafast Ti:sapphire amplifier (Newport-Spectra-Physics, Solstice) with a central wavelength of 800 nm, pulse lengths of 100 fs and a repetition rate of 1 kHz. One part of the output beam was used to seed an optical parametric amplifier (Newport-Spectra-Physics, TOPAS-C) as the source for the pump pulse with an attenuated energy of 200 nJ at wavelengths 520 and 575 nm and a pulse length of 140 fs. A small fraction of the Ti:sapphire output was focused into a moving calcium fluoride plate to produce a white light continuum between 350 nm and 800 nm, which acted as the probe pulse. Pump and probe were set to magic angle and spatially overlapped in the sample. After passing the sample the probe pulses were detected via a transient absorption spectrometer with a CMOS sensor (Ultrafast Systems, Helios). Part of the probe light pulse was used to correct for intensity fluctuations of the white light continuum. The relative temporal delay between pump and probe pulses was with a motorized, computer-controlled linear stage.

The fs time-resolved measurements for **RuOs** were performed on a system consisting of a Ti:sapphire amplifier (Legend-Elite, Coherent inc.), producing 35 fs pulses centred at 795 nm with a repetition rate of 1 kHz. The pump pulses centered at 520 and 670 nm were generated in a collinear optical-parametric amplifier (TOPAS-C, LightConversion Ltd.). The white light continuum between 450 and 700 nm to probe the sample is generated by focussing a part of the fundamental of the amplifier output into a sapphire plate. The pump pulses are delayed with respect to the probe pulses by means of an optical delay stage (maximum delay: 2 ns) and focused into the sample by a lens ($f = 1$ m), the energy of the pump pulses is attenuated to 1 μ J. Probe intensities fall into the range of a few hundred nJ. The repetition rate of the pump pulses is reduced to 500 Hz by a mechanical chopper and the polarization of the pump with respect to the probe pulses is set to the magic angle (54.7°) using a Berek compensator and a polarizer. The white light continuum is split into probe and reference. The probe pulse is focused onto the sample by a concave mirror ($f = 500$ mm) and spatially overlapped with the pump pulse. Probe and reference are collected by a detection system (Pascher Instruments, AB) consisting of a spectrograph (Acton, Princeton Instruments) equipped with a double-stripe diode array detector. The diode array is read out with the laser repetition rate and the signal (ΔA) is calculated from two consecutive probe pulses, corresponding to pump-on and pump-off conditions.

The chirp-corrected two-dimensional TA data matrix was fitted globally using a number of exponential functions, corresponding to a reaction scheme of consecutive first-order reactions. The wavelength-dependent preexponential factors correspond to the decay associated spectra (DAS). Global fitting of a more appropriate reaction scheme for the data of **RuFeRu** upon excitation at 520 nm was carried out using a home-written algorithm applying the Nelder-Mead algorithm⁴ as implemented in the `fminsearch` function in Scilab.⁵ The rate-constants are optimized via `fminsearch`. During fitting, the temporal evolution of the species concentrations

according to the reaction scheme is calculated iteratively, and the evolution associated spectra (species spectra, i.e. SAS) are calculated in a second step.

Steady-State Emission

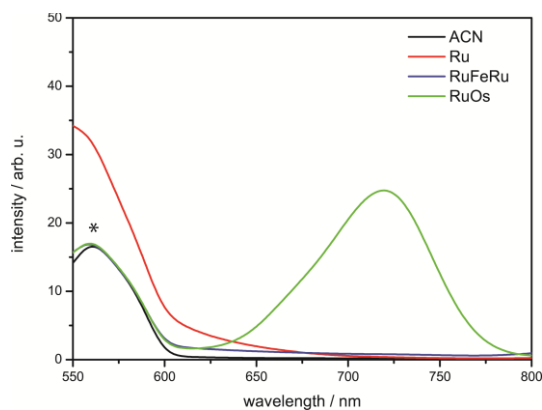


Figure S1: Emission spectra (solutions with identical optical density at the excitation wavelength) upon excitation at 488 nm. For comparison the background signal of the solvent is given additionally. Only **RuOs** displays clear $^3\text{MLCT}$ emission at room temperature in aerated acetonitrile. The weak signal for Ru below 700 nm is probably due to residual emission from LC states, which are also excited at 488 nm excitation^{6,7} (see Figure S2). The solvent Raman peak is marked with an asterisk.

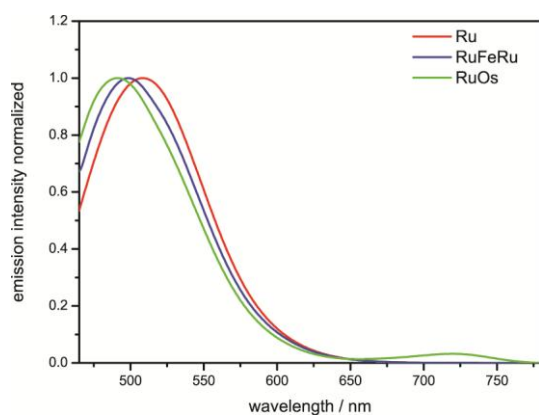


Figure S2: LC emission (spectra are normalized to the emission maximum) in aerated acetonitrile upon excitation at 425 nm (corresponding to the maximum of the LC absorption band). Only for **RuOs** weak $^3\text{MLCT}$ emission at 740 nm is observed additionally.

Absorption and Emission spectra of related Fe, Ru and Os complexes⁷

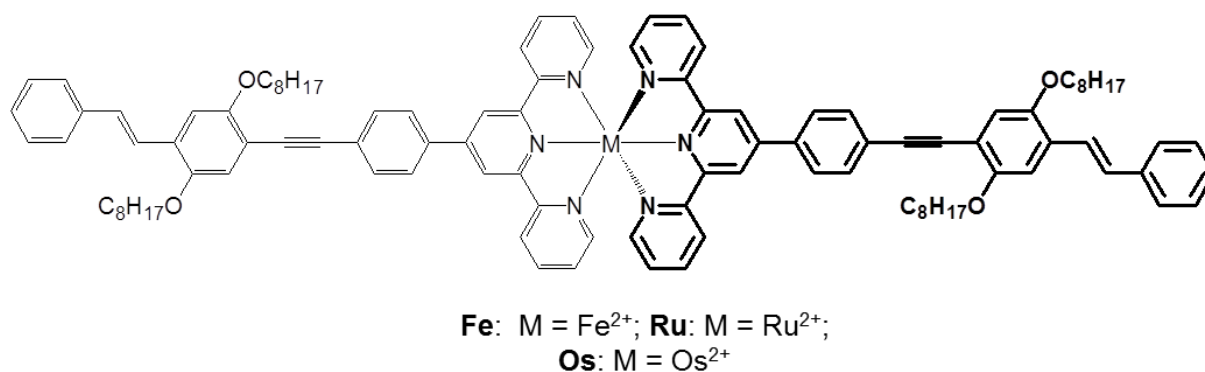


Figure S3: Structure of Ru, Fe and Os

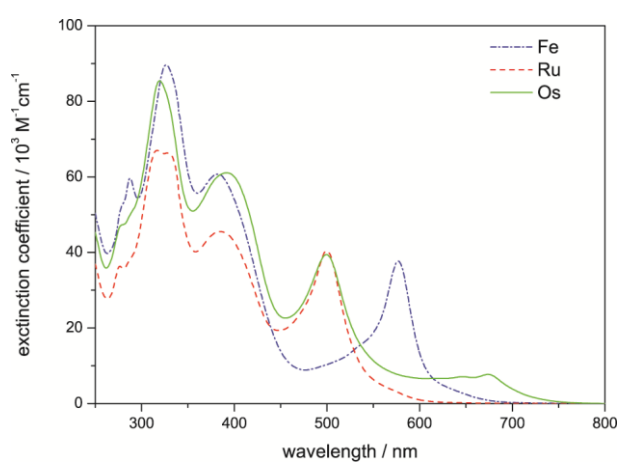


Figure S4: Absorption spectra of Fe, Ru and Os in THF

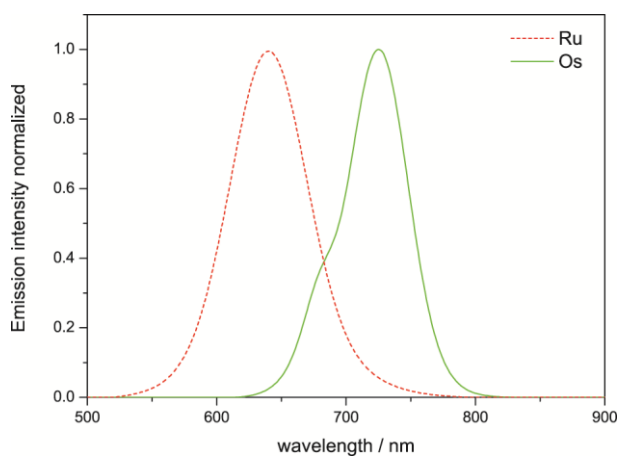


Figure S5: Emission spectra of Fe, Ru and Os in THF at room temperature, Fe shows no emission

Transient absorption measurements – ns regime

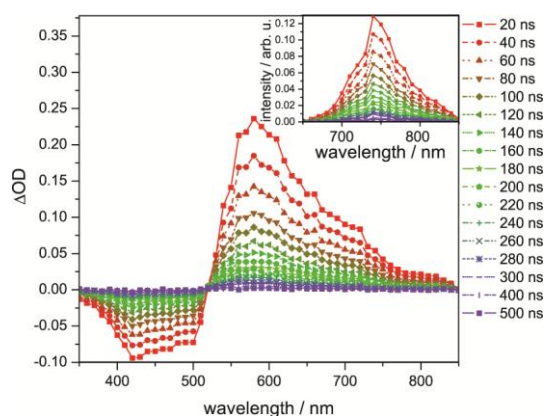


Figure S6: Transient spectra of **RuOs** upon excitation at 520 nm at selected delay times, the inset shows the emission spectra at chosen delay times.

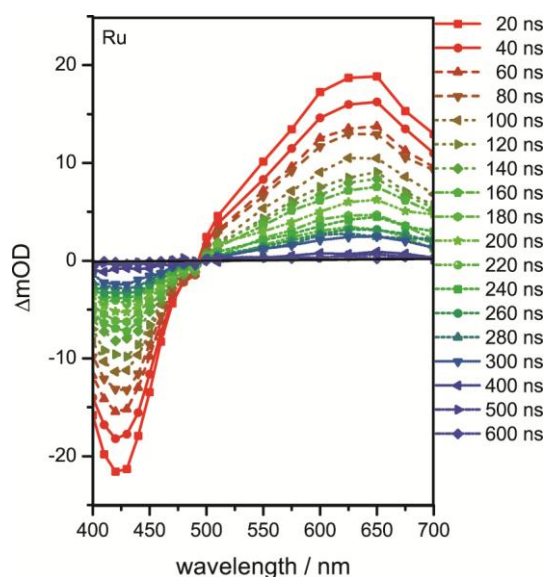


Figure S7: Transient spectra of **Ru** upon excitation at 520 nm at selected delay times.

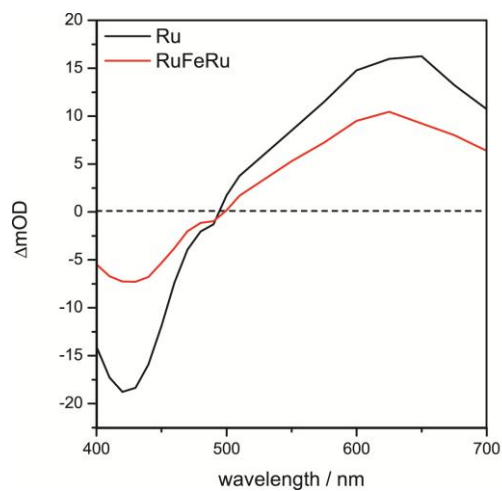


Figure S8: Comparison of the transient spectra of **Ru** and **RuFeRu** averaged between 20 and 60 ns after excitation at 520 nm.

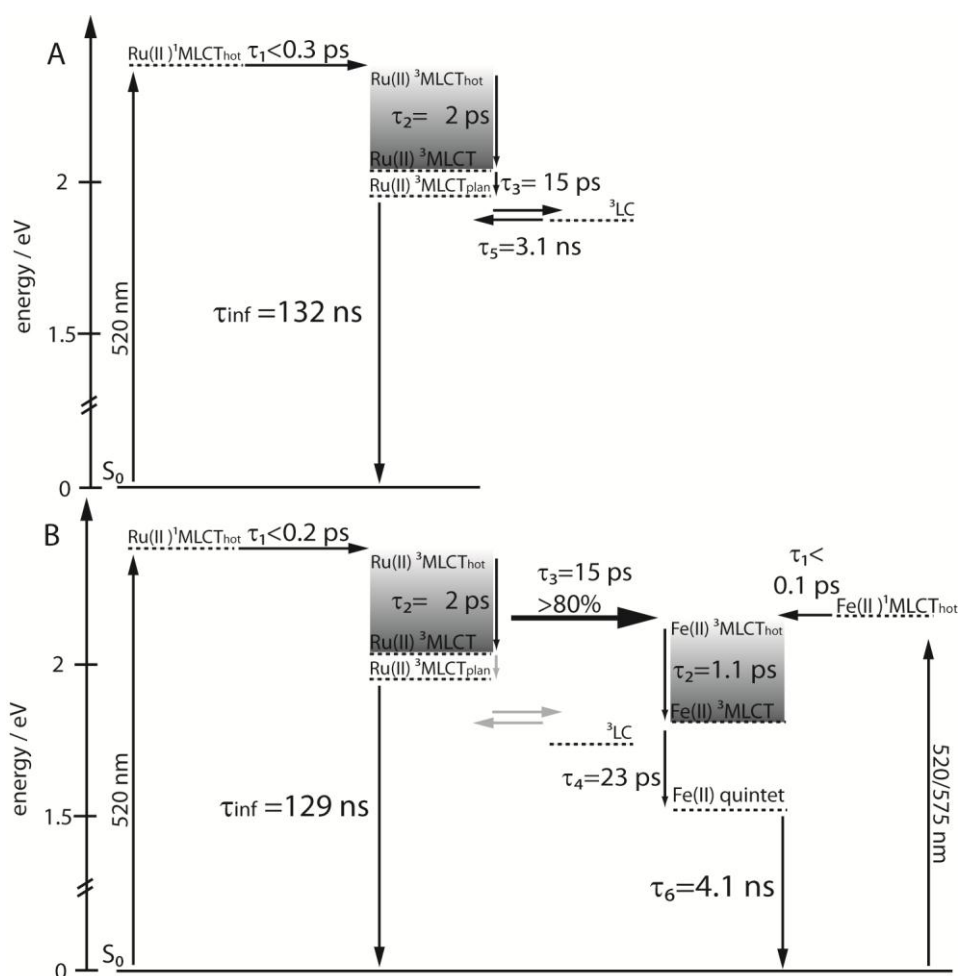
Transient absorption measurements – fs regime

A straight-forward fit of the data collected for **RuFeRu** with the kinetic components determined for the single metal centers, assuming a simple superposition of Ru(II) and Fe(II) centered photoinduced dynamics, was not sufficient to describe the observed temporal development of the signal (see Table S1 and Figure S9).

By applying a sum of exponential functions to describe the data at least 5 components and an additional infinite component are necessary (Figure S9 and Table S1). The two fastest processes τ_1 and τ_2 are superpositions of the $^3\text{MLCT}$ population and vibrational cooling at both the Fe(II) and the Ru(II) centers. Further, the processes corresponding to τ_6 and the infinite component can be easily identified by their spectral characteristics of their decay associated spectra (DAS) (Figure S11) by comparing with the DAS for the photoinduced processes of **Ru** and **RuFeRu** upon selective excitation of the Fe(II) center (Figure S10): τ_6 describes the decay of the quintet to the ground state. The infinite component represents the long-lived excited state at the Ru(II) center, which can also be observed in the ns time-resolved experiments (Figure S8 and S14). The very weak amplitude of this component compared to the data obtained for **Ru** is a first indication for the presence of an additional pathway depopulating the Ru(II) excited states in the presence of the Fe(II) center. These processes are probably faster than the equilibration between the Ru(II) $^3\text{MLCT}$ and the ^3LC state, hence the equilibration process escapes detection due to its very low amplitude (Figure S9 and S12). In contrast, the interpretation of the processes associated with $\tau_3 = 13$ ps and $\tau_4 = 44$ ps is not as straight forward. τ_3 is in the same temporal range as ligand planarization, which follows excitation at the Ru(II) center, but shows a completely different spectral shape for **RuFeRu** than for **Ru**. This component describes the decay of the Ru(II) spectral contributions parallel to a build-up of Fe(II) GSB, represented by the maximum in the DAS at 570 nm (Figure S11). Hence, this process can be interpreted as energy transfer between both centers. This transfer does not take place with unity quantum yield, i.e., some spectral

contributions from the Ru(II) excited states remain apparent at longer delay times. τ_4 could be assigned to the population of the Fe(II) quintet state, but it would be significantly decelerated (44 ps) compared to direct excitation of the iron center (23 ps). Further, it shows a rather high relative amplitude compared to excitation of only the Fe(II) center. There is no explanation for the seemingly deceleration of this process under changed excitation conditions at this point. Investigations addressing this matter are on the way.

The multi-exponential description is only correct for cascade kinetics or independent parallel relaxation at both centers.⁸ A comparison of the species associated spectra (SAS) of the photoinduced dynamics at the isolated Ru(II) and Fe(II) centers with the SAS for **RuFeRu** upon excitation at 520 nm resulting from the multi-exponential fit reveals, that while the sequential reaction model gives reasonable results for the kinetics at the single centers, for **RuFeRu** upon excitation at 520 nm the fit with the sequential model results in SAS, which correspond to a mixture of the different excited species, which are present (see Figure S13 and Figure 5 in the main text).⁸ Due to energy transfer depopulating the Ru(II) ³MLCT state and transferring population to Fe(II) ³MLCT states, the description with a sequential reaction scheme is not valid anymore. Hence, a modified model based on the processes and their respective timescales discussed above including the energy transfer between the metal centers was fitted numerically to the data (Scheme S1).



Scheme S1: Proposed relaxation schemes for **Ru** and **RuFeRu**, processes marked in gray are not directly observable, solid lines define energy levels with defined energetic positions, while dashed lines define excited states, the energy of which can only be indirectly inferred or depends on the excitation wavelength, processes in grey are not directly observed in the data

Table S1: global fit results of RuFeRu upon excitation at 520 nm with increasing number of exponentials

	$\tau_{1\text{Fe}}/$ ps	$\tau_{1\text{Ru}}/$ ps	$\tau_{2\text{Fe}}/$ ps	$\tau_{2\text{Ru}}/$ ps	$\tau_3/$ ps	$\tau_4/$ ps	$\tau_5/$ ps	$\tau_6/$ ps	
RuFeRu_520 nm									
1 component					35				Inf
2 components	0.9				23				Inf
3 components	0.8				26			4100	Inf
4 components	0.8				12	44		4300	Inf
5 components	0.2		1.3		13	44		4300	Inf
6 components	0.2		1.4		13	44	230	4100	Inf
Fixed ^a	0.1	0.3	1.1	2.0	15	23	3100	4100	Inf
Model ^b	0.2		1.4		15	56		4200	Inf
RuFeRu_570 nm	0.1		1.1			23		4100	
Ru_520 nm		0.3		2.0	15		3100		Inf

a) fit with the kinetic components determined for the single metal centers (**RuFeRu** excitation 570 nm, **Ru** excitation 520 nm), assuming a simple superposition of Ru(II) and Fe(II) centered photoinduced dynamics

b) numerical fit, model described in the main text (Scheme 1, and Scheme S1)

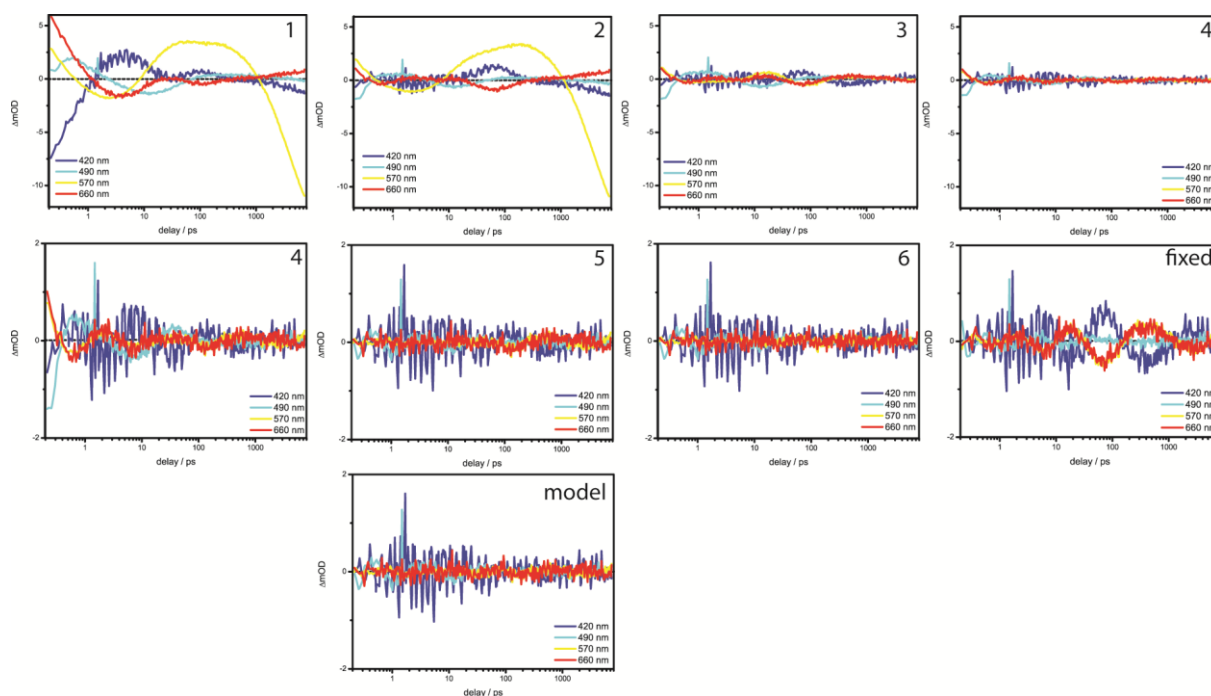


Figure S9: Residuals of the global fit with varying number of exponentials (see table S1) for **RuFeRu** excited at 520 nm, also the residuals of the fit with fixed time constants determined for **Ru** and upon selective excitation of the Fe(II) center of **RuFeRu** and the fit with the modified model are included.

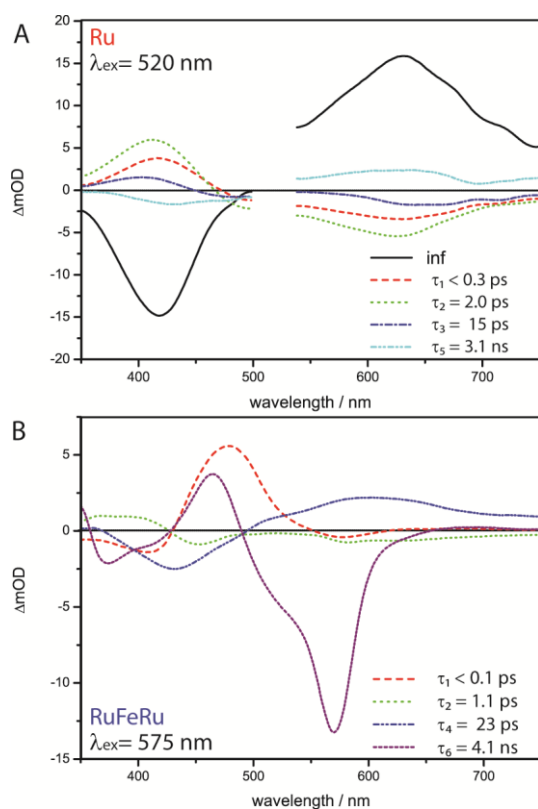


Figure S10: Decay associated spectra (DAS) and respective time constants resulting from a multi-exponential global fit of (A) **Ru** upon excitation at 520 nm and (B) **RuFeRu** upon excitation 575 nm, representing the characteristic photoinduced dynamics and spectral characteristics at the Ru(II) and the Fe(II) center, respectively. Planarization and equilibration processes with the 3LC states can be identified by comparison to related structures by their characteristic DAS^{7,9}

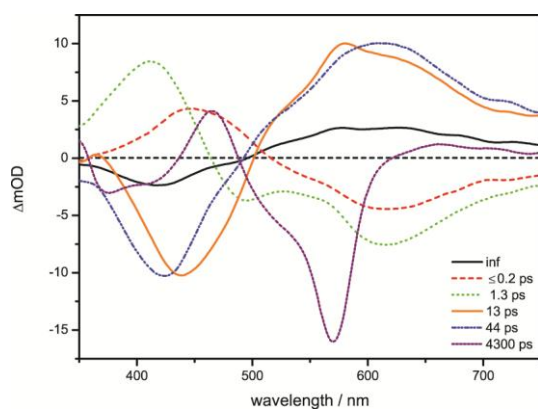


Figure S11: DAS of the multi-exponential fit of **RuFeRu** with 5 exponentials upon excitation at 520 nm.

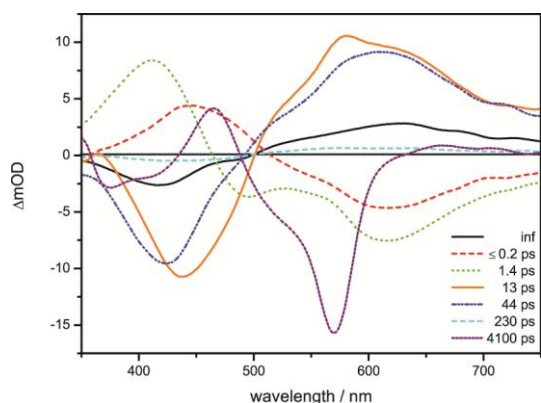


Figure S12: DAS of the multi-exponential fit with 6 exponentials of **RuFeRu** upon excitation at 520 nm. The component with a time constant of 230 ps fits spectrally to the equilibration process, but shows only very weak contributions, hence can only be determined with high inaccuracy.

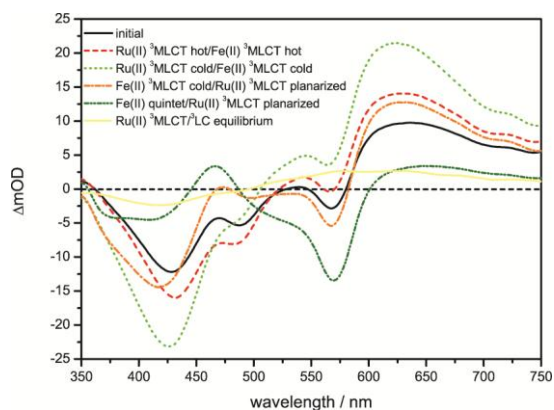


Figure S13: SAS from the multi-exponential fit (sequential model) with 5 exponentials of **RuFeRu** upon excitation at 520 nm. From comparison with the SAS resulting from a sequential fit of the dynamics of the centers selectively excited it is apparent, that the SAS determined from the multi-exponential fit are superpositions of these SAS of the single centers. This indicates that the model needs to be modified.

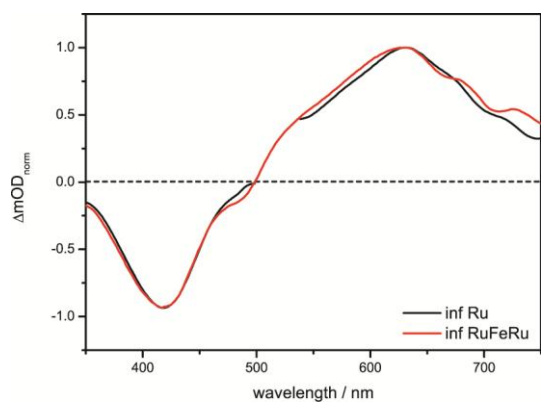


Figure S14: Comparison of the long-lived components (normalized representation) in the fs time-resolved measurements of **Ru** and **RuFeRu** upon excitation at 520 nm illustrating the identity of the long-lived state in **Ru** and **RuFeRu**.

Estimation of the energy transfer efficiency in **RuFeRu**

The fs time-resolved measurements were performed under identical excitation conditions (wavelength and intensity).

Assumption 1: extinction coefficients of the Ru(II) ¹MLCT transitions in the ground state are not significantly changed upon coordination of the Fe(II) center.

Then the part of Ru(II) excitation in **RuFeRu** can be determined by regarding the absorption spectrum of **RuFeRu** as sum of two times the absorptions spectrum of **Ru** plus the unknown absorption spectrum of the iron center. This leads to an initial excitation ratio at 520 nm of approximately 3(Ru):1(Fe).

Assumption 2: Excited state extinction coefficients are also not changed significantly upon coordination of the Fe(II) center.

The ratio of signal intensity of the long-lived component is determined to 1(**Ru**):0.16(**RuFeRu**). This means that 84% of signal intensity is quenched by energy transfer from the Ru to the Fe center. This value would hold true if the optical intensities of the samples were adjusted in a way that both show equal optical density of the Ru ¹MLCT transition. The optical densities at 520 nm were 0.12 for **Ru** and 0.21 for **RuFeRu**. Regarding the excitation ratio determined above this leaves an optical density for the Ru ¹MLCT transitions of 0.15 in **RuFeRu**, which is slightly too high. Assuming that a sample of higher optical density gives a higher transient signal, the determined value for the efficiency of energy transfer defines a lower limit, as the signal detected for **RuFeRu** is even too high.

From this short estimation we conclude that we can state that energy transfer occurs with at least 80 % efficiency in **RuFeRu**.

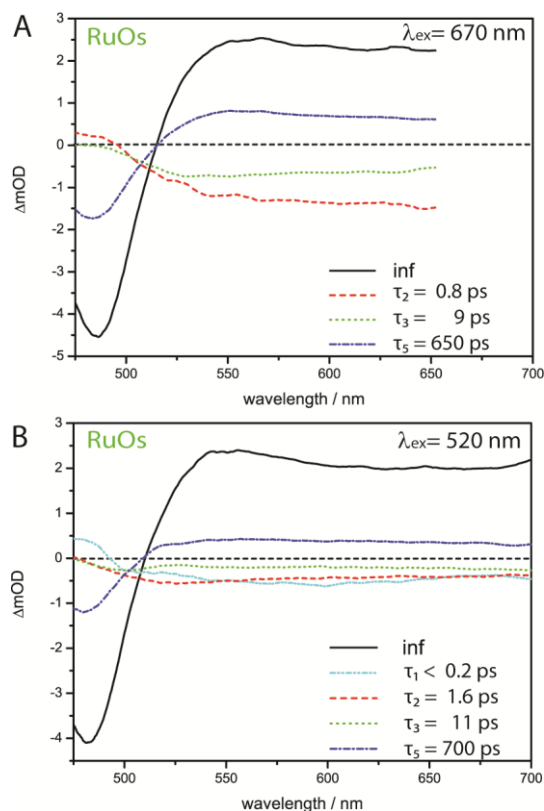


Figure S15: DAS and respective time constants resulting from a multi-exponential global fit for **RuOs** (A) upon excitation at 670 nm and (B) 520 nm.

References

1. A. Winter, C. Friebe, M. D. Hager and U. S. Schubert, *Eur. J. Org. Chem.*, 2009, 801-809.
2. B. Schulze, D. Escudero, C. Friebe, R. Siebert, H. Görls, S. Sinn, M. Thomas, S. Mai, J. Popp, B. Dietzek, L. Gonzalez and U. S. Schubert, *Chem.-Eur. J.*, 2012, 18, 4010-4025.
3. D. F. Zigler, M. T. Mongelli, M. Jeletic and K. J. Brewer, *Inorg. Chem. Commun.*, 2007, 10, 295-298.
4. J. A. Nelder and R. Mead, *The Computer Journal*, 1965, 7, 308-313.
5. S. E. (2012). *Scilab: Free and Open Source software for numerical computation (OS, Version 5.XX) [Software]*. , Available from: <http://www.scilab.org>.
6. R. Siebert, A. Winter, B. Dietzek, U. S. Schubert and J. Popp, *Macromol. Rapid Commun.*, 2010, 31, 883-888.
7. R. Siebert, A. Winter, U. S. Schubert, B. Dietzek and J. Popp, *Phys. Chem. Chem. Phys.*, 2011, 13, 1606-1617.
8. I. H. M. van Stokkum, D. S. Larsen and R. van Grondelle, *Biochim. Biophys. Acta*, 2004, 1658, 262-262.
9. R. Siebert, C. Hunger, J. Guthmüller, F. Schlütter, A. Winter, U. S. Schubert, L. Gonzalez, B. Dietzek and J. Popp, *J. Phys. Chem. C*, 2011, 115, 12677-12688.